## The Harrow-Hassidim-Lloyd algorithm with qutrits

Tushti Patel<sup>1,2,\*</sup> and V. S. Prasannaa<sup>1,3,†</sup>

<sup>1</sup>Centre for Quantum Engineering, Research and Education, TCG CREST, Kolkata 700091, India <sup>2</sup>Department of Physics, IIT Tirupati, Chindepalle, Andhra Pradesh 517619, India <sup>3</sup>Academy of Scientific and Innovative Research (AcSIR), Ghaziabad 201002, India

We extend the Harrow-Hassidim-Lloyd (HHL) algorithm, which is well-studied in the qubit framework, to its qutrit counterpart (which we call qutrit HHL, as opposed to qubit HHL, which is HHL using qubits). We design the circuit for the algorithm and develop a program for its implementation. We test HHL with qutrits for simple matrices and verify the results against the expected outcomes. We apply the algorithm to quantum chemistry, and in particular, to the potential energy curve calculations of the model problem of the hydrogen molecule in the split valence basis. We compare the number of qudits and the number of gates required between qubit and qutrit HHL implementations. In general, we find that for a fixed precision, the qutrit HHL circuit requires fewer number of qudits and comparable number of two-qudit gates than its qubit counterpart.

## I. INTRODUCTION

The Harrow-Hassidim-Lloyd (HHL) algorithm [1] is a quantum algorithm designed to solve systems of linear equations of the form  $A\vec{x} = \vec{b}$ , where A is a matrix of dimension  $N \times N$ , while  $\vec{x}$  and  $\vec{b}$  are vectors of dimension  $N \times 1$ . HHL finds an approximation to  $|x\rangle = A^{-1}|b\rangle$ , where  $|b\rangle$  is a suitably encoded version of  $\vec{b}$ . It is one of the few quantum algorithms that, in principle, promises an exponential advantage in system size. It has numerous applications in a wide variety of problems, such as portfolio optimization [2], security against cyberattacks on a quantum computer [3], fluid dynamics [4], power flow [5], and solving the Poisson equation [6]. Recently, it was identified that HHL can be used to solve chemistry problems [7–9] in addition to the existing variational quantum eigensolver (VQE) [10] and quantum phase estimation (QPE) [11] methods for quantum chemical applications. Quantum chemistry is identified to be one of the killer applications of quantum computing, and the analysis by the authors of Reference [8, 12] show that  $\kappa$  (condition number of A) and s (the number of non-zero entries in the row with the maximum number of non-zero entries) scaling are favorable (polylogarithmic in number of spin orbitals) within the limited molecules they consider. Furthermore, the system size, that is, the size of the A matrix itself, scales polynomially in the number of spin orbitals. Therefore, one can expect a polynomial advantage with HHL applied to chemistry.

All of the above discussed works involve qubits. Recent works have identified that using qudits for quantum al-

gorithms can have potential advantages over their qubit counterparts [13, 14]. Several algorithms like Deutsch-Josza, Bernstein-Vazirani, quantum Fourier transform (QFT), QPE, etc, have been discussed in the qudit framework [15]. Despite the large volume of ongoing research in quantum algorithms and computing, there remains a relative paucity of literature on higher-dimensional qudits, and in particular, qutrits, where a qutrit has an additional quantum level relative to a qubit, but which is a natural extension to consider. Furthermore, in view of some of the recent advances in qutrit hardware [14, 16, 17], it is timely to explore the domain of quantum algorithms with qutrits. Therefore, given the potential of HHL for offering advantage across a wide variety of problems and the timely need to investigate quantum algorithms using gutrits, we extend the HHL algorithm to the gutrit framework (which we shall term as qutrit HHL hereafter). Furthermore, we consider quantum chemistry as a pilot application for qutrit HHL and to that end, carry out calculations to generate the potential energy curve for the model system of  $H_2$  in a split valence basis. This is followed by a comparative analysis of the costs involved between qubit and qutrit HHL calculations. To the best of our knowledge, one previous work proposes qutrit HHL, but only presents a preliminary circuit design [18].

The subsequent sections are organized as follows: Section II introduces the HHL algorithm for qubits. Following a primer on ternary logic and qutrit gates in Sections III A and III B respectively, we move to our qutrit HHL implementation is discussed in Section III C. We then provide a brief introduction to the quantum chemistry application, in which we solve for the correlation energy using HHL (Section IV). We then discuss results from our numerical simulations in Section V, which include toy matrices (Section V A) and quantum chemistry (Section

 $<sup>^*</sup>$  tushti.oficial@gmail.com

<sup>†</sup> srinivasaprasannaa@gmail.com

VB). We then carry out a comparative analysis between qubits and qutrits in Section VI, where we discuss estimates for the number of qudits required (Section VIA) and the number of two-qudit gates incurred for HHL calculations in the qubit and qutrit cases (Section VIB). We finally conclude in Section VII.

#### II. THE HHL ALGORITHM

The HHL algorithm is discussed in detail, for example, in Reference [19], but here we provide only the relevant details that we would need for a subsequent gutrit extension of the algorithm. Figure 1 gives a schematic quantum circuit representation of the algorithm. The  $N \times 1$  dimensional vector,  $\vec{b}$ , which is an input to the algorithm, is encoded in an m-dimensional normalized quantum state  $|b\rangle_m$  in the state register via amplitude encoding such that  $2^m = N$  for qubits. On the other hand, the matrix A is used in the circuit as a part of a controlled-unitary of the form  $CU = C e^{iAt}$ , where  $U = e^{iAt}$  for an appropriately chosen scalar, t. As the figure shows, the HHL circuit broadly comprises of three parts - (a) QPE, (b) Controlled-rotation, and (c) Inverse of QPE. These steps are followed by measurement and post-selection. The above-mentioned controlled-unitaries, which are controlled on a set of  $n_r$  clock register qubits, are used for quantum phase estimation. At the end of the QPE module, the eigenvalues of A are stored in the clock register with a precision of  $n_r$  digits. The parametrized controlled-rotation module,  $CR(\theta)$ , implements inversion of eigenvalues using an ancillary qubit that we call the HHL ancilla for brevity. The inverse QPE module is then applied in order to disentangle the clock register from the rest of the system. Post-selection of  $|1\rangle$  in the HHL ancilla results in a quantum state  $|\tilde{x}\rangle$  in the state register, which is proportional to the required  $\vec{x}$ . For any application, where some feature of  $\vec{x}$  is to be evaluated, an additional module can be appended to the HHL circuit. For example, if the application of interest to us is quantum chemistry and we intend to compute molecular energies using HHL, then a controlled-swap test circuit module could be added at the end of the HHL circuit, as discussed in Reference [7].

## III. HHL WITH QUTRITS

In this section, we discuss the HHL algorithm using qutrits in detail.

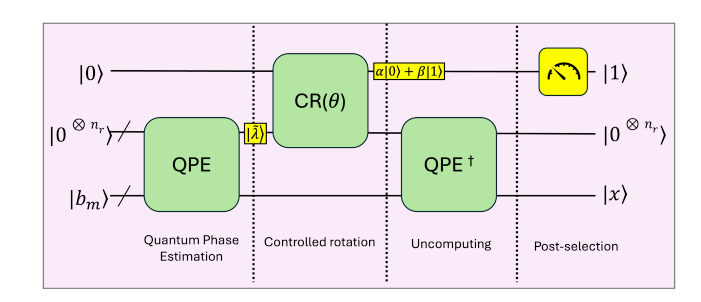


Figure 1: Schematic representation of the HHL algorithm.

### A. A brief introduction to ternary logic

We begin our discussion with a concise introduction to ternary logic. Ternary logic is a multi-valued logic system that extends the binary system of logic by adding a third state '2' to  $\{0,1\}$ . Thus, the computational basis for a ternary quantum state would be  $\{|0\rangle,|1\rangle,|2\rangle\}$ . A general qutrit state can be defined as  $|\psi\rangle=\alpha_0|0\rangle+\alpha_1|1\rangle+\alpha_2|2\rangle$  where  $|\alpha_0|^2+|\alpha_1|^2+|\alpha_2|^2=1$ . Similarly, an n-qutrit state would have  $3^n$  different possible states. In terms of the state vector notation, we can represent the computational basis vectors as -

$$|0\rangle = \begin{pmatrix} 1\\0\\0 \end{pmatrix}, \quad |1\rangle = \begin{pmatrix} 0\\1\\0 \end{pmatrix}, \quad \text{and} \quad |2\rangle = \begin{pmatrix} 0\\0\\1 \end{pmatrix}.$$

## B. Basic gates for qutrits

In this study, we work with a palette of one- and two-qutrit gates. This includes the one- and two-qutrit Clifford gates introduced in Reference [20], that is, the qutrit equivalents of the Pauli X and Z gates, and the CX gate. We also pick the H gate, the phase gate, and planar rotation gate, along with their controlled counterparts of the latter two [15]. Our choice of gates to build the qutrit HHL circuit is motivated by convenience in circuit construction. Thus, we describe in detail only those gates.

## 1. One-qutrit gates

1. Increment gate (X): The qutrit X gate increments a computational basis state of the qutrit in cyclic

order. It is specified in its matrix representation as

$$X = \begin{pmatrix} 0 & 0 & 1 \\ 1 & 0 & 0 \\ 0 & 1 & 0 \end{pmatrix}.$$

In the outer product notation,

$$X = |1\rangle\langle 0| + |2\rangle\langle 1| + |0\rangle\langle 2|.$$

The action of this gate can be described as follows

$$X|0\rangle = |1\rangle$$

$$X|1\rangle = |2\rangle$$

$$X|2\rangle = |0\rangle.$$

2. Z gate:

$$Z = \begin{pmatrix} 1 & 0 & 0 \\ 0 & \omega & 0 \\ 0 & 0 & \omega^2 \end{pmatrix}.$$

In the outer product notation,

$$Z = |0\rangle\langle 0| + \omega|1\rangle\langle 1| + \omega^2|2\rangle\langle 2|,$$

where  $\omega = e^{\frac{2\pi i}{3}}$  is the third root of unity.

The action of this gate can be described as follows

$$Z|0\rangle = |0\rangle$$

$$Z|1\rangle = \omega|1\rangle$$

$$Z|2\rangle = \omega^2|2\rangle.$$

3. Hadamard gate (H):

$$H = \frac{1}{\sqrt{3}} \begin{pmatrix} 1 & 1 & 1\\ 1 & \omega & \omega^2\\ 1 & \omega^2 & \omega \end{pmatrix}.$$

In the outer product notation,

$$H = \frac{1}{\sqrt{3}} \sum_{j,k \in \{0,1,2\}} \omega^{j \cdot k} |j\rangle\langle k|.$$

The action of this gate can be described as follows

$$\begin{split} H|0\rangle &= \frac{|0\rangle + |1\rangle + |2\rangle}{\sqrt{3}} \\ H|1\rangle &= \frac{|0\rangle + \omega|1\rangle + \omega^2|2\rangle}{\sqrt{3}} \\ H|2\rangle &= \frac{|0\rangle + \omega^2|1\rangle + \omega|2\rangle}{\sqrt{3}}. \end{split}$$

4. Phase gate  $(P_l)$ :

$$P_l = \begin{pmatrix} 1 & 0 & 0 \\ 0 & e^{\frac{2\pi i}{3^l}} & 0 \\ 0 & 0 & e^{\frac{4\pi i}{3^l}} \end{pmatrix}.$$

in the outer product notation,

$$P_l = |0\rangle\langle 0| + e^{\frac{2\pi i}{3^l}} |1\rangle\langle 1| + e^{\frac{4\pi i}{3^l}} |2\rangle\langle 2|.$$

The action of this gate can be described as follows

$$P_l|0\rangle = |0\rangle$$

$$P_l|1\rangle = e^{\frac{2\pi i}{3^l}}|1\rangle$$

$$P_l|2\rangle = e^{\frac{4\pi i}{3^l}}|2\rangle.$$

5. Planar rotation gate  $(R_{ij}(\theta))$ : This gate performs rotation about the axis perpendicular to the ij plane. For example, we may perform a rotation in the  $|0\rangle - |1\rangle$  plane,

$$R_{01}(\theta) = \begin{pmatrix} \cos(\frac{\theta}{2}) & -\sin(\frac{\theta}{2}) & 0\\ \sin(\frac{\theta}{2}) & \cos(\frac{\theta}{2}) & 0\\ 0 & 0 & 1 \end{pmatrix}.$$

The action of this gate can be described as follows

$$R_{01}(\theta)|0\rangle = \cos\left(\frac{\theta}{2}\right)|0\rangle + \sin\left(\frac{\theta}{2}\right)|1\rangle$$

$$R_{01}(\theta)|1\rangle = -\sin\left(\frac{\theta}{2}\right)|0\rangle + \cos\left(\frac{\theta}{2}\right)|1\rangle$$

$$R_{01}(\theta)|2\rangle = |2\rangle.$$

### 2. Two-qutrit gates

1. Controlled increment (CX): The controlled increment gate increments the state of the target qutrit depending on the control qutrit. This gate is also called the SUM gate as the operation is equivalent to a modulo 3 addition. The CX gate is defined as

$$CX|j,k\rangle = |j+k \pmod{3}\rangle,$$

where j is the control qutrit and k is the target qutrit. In general, the action of the CX gate can

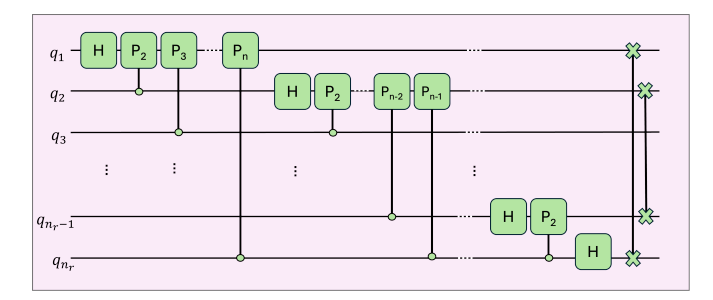


Figure 2: Quantum Fourier transform circuit for qutrits.

be described as -

$$CX|0,k\rangle = |0\rangle|k\rangle$$

$$CX|1,k\rangle = |1\rangle X|k\rangle$$

$$CX|2,k\rangle = |2\rangle X^{2}|k\rangle,$$

where  $|k\rangle$  is any qutrit state, and the action of the X gate is already defined in the list of single qutrit gates.

2. Controlled  $P_l$  gate: The action of the controlled  $P_l$  gate is described as -

$$CP_l|0,k\rangle = |0\rangle|k\rangle$$
  
 $CP_l|1,k\rangle = |1\rangle P_l|k\rangle$   
 $CP_l|2,k\rangle = |2\rangle P_l^2|k\rangle$ .

3. Generalized controlled  $R_{ij}(\theta)$ : In this construction,  $R_{ij}(\theta)$  gate acts on the target qutrit only if the state of the control qutrit is equal to  $|m\rangle$ , where m is either 0, 1, or 2.

# C. Qutrit HHL: working principles and quantum circuit

The HHL algorithm has been described briefly in Section II. In this section, we discuss our extension to the qutrit framework. The general problem statement remains the same, that is, solving a system of linear equations of the form  $A\vec{x}=\vec{b}$ . The  $\vec{b}$  of dimension  $N\times 1$  is encoded in a state register containing m qutrits using amplitude encoding such that  $3^m=N$ . In addition to the state register, we have a clock register comprising of  $n_r$  qutrits. These are useful for capturing the eigenvalues via the QPE module. Lastly, we have a single qutrit ancilla, also known as the HHL ancilla, which will be used for eigenvalue inversion through the controlled rotation module.

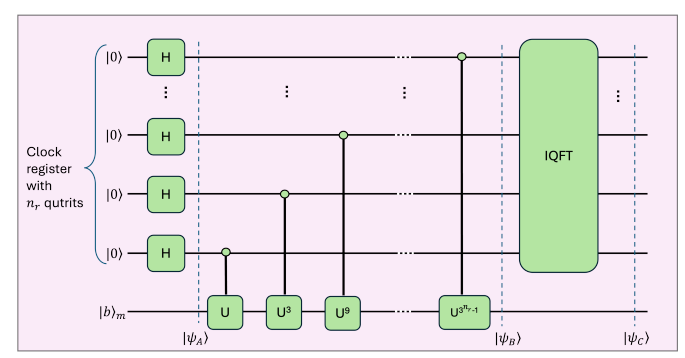


Figure 3: Quantum phase estimation circuit for qutrits.

We begin by discussing the quantum Fourier transform (QFT) module, since its inverse (IQFT) occurs in the QPE module. Figure 2 gives the circuit for QFT. Although the circuit is similar to that for qubits, the gate definitions are modified in the qutrit framework. We define the generalized  $P_l$  gate for qutrits as specified in Section III B. Implementing the QFT circuit on a general qutrit state  $|j_1, j_2, \ldots j_n\rangle$ , we obtain -

$$QFT |j_1, j_2, \dots j_n\rangle = \frac{1}{3^{n/2}} \sum_{k=0}^{3^n - 1} e^{\frac{2\pi i(j,k)}{3^n}} |k_1, k_2, \dots k_n\rangle.$$

The circuit for the QPE module is given in Figure 3. QPE consists of mainly controlled unitaries, with the unitary matrix of the form  $U=e^{iAt}$  where A is the Hermitian matrix that occurs the system of linear equations to be solved, and t is a problem-dependent constant such that  $U(\sum_{i=0}^{3^m-1}b_i|u_i\rangle)=\sum_{i=0}^{3^m-1}b_ie^{2\pi i\phi_i}|u_i\rangle$  where  $\phi_i\mathbf{s}\in[0,1]$  are the eigenvalues of A. The clock registers are initially all in state  $|0\rangle$ . First, all the clock registers are acted upon by the ternary Hadamard gates resulting in -

$$|\psi_A\rangle = \left(\frac{|0\rangle + |1\rangle + |2\rangle}{\sqrt{3}}\right)^{\otimes n_r} \otimes |b\rangle_m.$$

Upon the application of the series of controlled unitaries shown in Figure 3, we obtain

$$|\psi_{B}\rangle = \sum_{i=0}^{3^{m}-1} b_{i} \left( \frac{|0\rangle + e^{3^{n_{r}-1} 2\pi i \phi_{i}} |1\rangle + e^{3^{n_{r}-1} 4\pi i \phi_{i}} |2\rangle}{\sqrt{3}} \right) \otimes \left( \frac{|0\rangle + e^{3^{n_{r}-2} 2\pi i \phi_{i}} |1\rangle + e^{3^{n_{r}-2} 4\pi i \phi_{i}} |2\rangle}{\sqrt{3}} \right) \otimes \dots \otimes \left( \frac{|0\rangle + e^{2\pi i \phi_{i}} |1\rangle + e^{4\pi i \phi_{i}} |2\rangle}{\sqrt{3}} \right) \otimes |u_{i}\rangle_{m}.$$

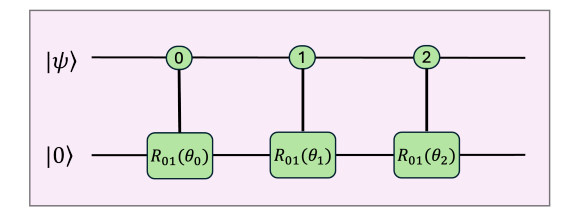


Figure 4: Uniform controlled-rotation circuit for 1 control qutrit.

Substituting  $\phi_i$ s in the form  $\tilde{\phi}_i = 0.j_1j_2...j_{n_r}^{(i)}$ , we obtain an expression equivalent to that of QFT, and hence the inverse QFT module takes the eigenvalues of A from the phase to the qutrit state. The precision is, of course, limited by the number of clock register qutrits used and the resultant state after the QPE module  $|\psi_C\rangle = \sum_{i=0}^{3^m-1} b_i |\tilde{\phi}_i\rangle \otimes |u_i\rangle_m$ . Reference [15] briefly describes the QFT and QPE modules for higher-dimensional qudits, in general. We have worked them out in detail for the specific case of qutrits.

Next, we have the parametrized controlled-rotation module, which is used for eigenvalue inversion. Rotations in general could be quite complex in a qutrit framework, and for the purposes of our HHL algorithm, we choose to use planar rotations, that is, a rotation of any two of the three orthogonal gutrit basis states. Without loss of generality, we consider  $|0\rangle$  and  $|1\rangle$  for our rotations (any other combination can be used equivalently). The rotation gate as well as the controlled-rotation gates have been described in detail in Section IIIB. The simple example circuit shown in Figure 4 serves as an illustration of the workings of uniformly controlled rotations. We assume that the control qutrit is in a general state  $|\psi\rangle = \alpha_0|0\rangle +$  $\alpha_1|1\rangle + \alpha_2|2\rangle$ . The action of the three controlled-rotation gates (UCR) can be described in the outer product notation as  $|0\rangle\langle 0|\otimes R_{01}(\theta_0)+|1\rangle\langle 1|\otimes R_{01}(\theta_1)+|2\rangle\langle 2|\otimes R_{01}(\theta_2)$ . Therefore,

$$\begin{split} UCR(|\psi\rangle \otimes |0\rangle) &= \sum_{i=0}^{2} \alpha_{i} |i\rangle \\ &\otimes \left( \sqrt{1 - \sin^{2} \left(\frac{\theta_{i}}{2}\right)} |0\rangle + \sin \left(\frac{\theta_{i}}{2}\right) |1\rangle \right). \end{split}$$

Substituting for thetas  $\theta_i = 2 \sin^{-1} \left( \frac{C}{\bar{\phi_i}} \right)$ , where C is a suitably chosen constant which is generally taken as the

minimum eigenvalue of A, we get

$$UCR(|\psi\rangle\otimes|0\rangle) = \sum_{i=0}^{2} \alpha_{i}|i\rangle\otimes\left(\sqrt{1-\left(\frac{C}{\tilde{\phi}_{i}}\right)^{2}}|0\rangle + \frac{C}{\tilde{\phi}_{i}}|1\rangle\right).$$

Thus, the coefficient of  $|1\rangle$  is the required inverse of the eigenvalues. The same logic can be extended to multiple control qutrits with multi-controlled rotation gates. The clock register acts as the set of control qutrits.

Lastly, the inverse QPE module and measurement of the HHL ancilla qutrit followed by post-selection of  $|1\rangle$  are implemented to obtain  $|\tilde{x}\rangle$  in the state register, which is proportional to the required  $\vec{x}$  upto known constants.

## IV. APPLICATION OF QUTRIT HHL FOR MOLECULAR GROUND-STATE ENERGY CALCULATIONS

In this section we discuss the application of qutrit HHL to quantum chemistry problems. For this purpose, we use the linearized form of coupled cluster equations [21] as our system of linear equations -

$$\sum_{q} \langle \chi_p | H | \chi_q \rangle t_q = -\langle \chi_p | H | \Phi_0 \rangle , \forall p$$
 (1)

where,

- $|\Phi_0\rangle$  is the Hartree-Fock determinant,
- $|\chi_p\rangle$  represents the  $p^{th}$  excited state determinant,
- $|\chi_q\rangle$  is the  $q^{th}$  excited state determinant,
- ullet H is the normal-ordered Hamiltonian operator, and
- $t_q$  is the  $q^{th}$  cluster amplitude.

We see that equation 1 takes the form of a system of linear equations, with the vector of cluster amplitudes being the unknown vector,  $\vec{x}$ .

The quantity of interest to us is the correlation energy which is given by -

$$\begin{split} E_{corr} &= \langle \Phi_0 | H | \chi_p \rangle t_p \\ &= -\vec{b}^\dagger A^{-1} \vec{b} \\ &= -k |\langle b | x \rangle|, \end{split}$$

where  $k = ||x\rangle_{un}|| ||b\rangle_{un}||^2$ . We note that we already know  $|b\rangle_{un}$ , while  $|x\rangle_{un}$  can be obtained from P(1) on the HHL ancilla qutrit. The molecular simulation problem is discussed in Reference [7], one may refer to it and the

references therein for detailed equations and derivations. Although we are interested in energy for the purposes of this work, one can in principle use the HHL algorithm for computing other molecular properties in the qubit or qutrit framework with an appropriate circuit module appended at the end of the HHL quantum circuit.

The controlled-swap circuit can be appended to the HHL quantum circuit to compute the overlap of the two quantum states  $|b\rangle$  and  $|x\rangle$  [22]. In the case of qubits, the absolute value of the overlap is extracted using the expression  $P(0) = \frac{1}{2} \left(1 + |\langle b|x\rangle|^2\right)$ . On the other hand, for qutrit swap test, we allow the controlled-swap gate to swap the state only when it is controlled on  $|2\rangle$ , we can obtain the absolute value of the overlap as  $P(0) = \frac{1}{9} \left(5 + 4|\langle b|x\rangle|^2\right)$ . We add that Reference [7] uses a destructive version of the controlled-swap test, while we use the traditional version of the circuit.

### V. RESULTS

### A. Testing with toy matrices

We use the Berkeley Quantum Synthesis Toolkit (BQSKit) software development kit [23] to develop our qutrit HHL codes and to perform the simulations, since it supports computation with higher-dimensional qudits. We also develop our qubit HHL codes in the same framework so that we can then compare the results from qubit and qutrit HHLs on an equal footing. In order to test our implementation, we carry out qutrit HHL calculations on toy matrices. We begin with a simple  $3\times 3$  diagonal matrix A, and  $\vec{b}$  given by

$$A = \begin{pmatrix} 0.2 & 0 & 0\\ 0 & 0.5 & 0\\ 0 & 0 & 0.8 \end{pmatrix} \text{ and } \vec{b} = \frac{1}{\sqrt{3}} \begin{pmatrix} 1\\ 1\\ 1 \end{pmatrix}$$
 (2)

respectively. We note that our choice for  $\vec{b}$  is normalized for qutrit states, and can directly be amplitude encoded as  $|b\rangle = \frac{1}{\sqrt{3}}(|0\rangle + |1\rangle + |2\rangle)$ . This state can be achieved using a single qutrit Hadamard gate. The statevector results obtained for this calculation using qutrit HHL for different values of  $n_r$  are given in Table I. We see that our result for  $\vec{x}$  is in good agreement with the solution vector obtained classically when  $n_r = 6$ .

We also carry out a simple calculation with another  $3 \times 3$  toy matrix, but this time non-diagonal. Our choice for the A matrix and  $\vec{b}$  are given by

Table I: Results from executing the qutrit HHL algorithm for the toy A matrix and  $\vec{b}$  described in equation (2), for different numbers of QPE clock register qubits. PFD refers to the percentage fraction difference between our result and the expected result obtained classically.

| $n_r$ | $ec{x}$            | $ \langle b x\rangle $ | PFD (%) |
|-------|--------------------|------------------------|---------|
| 3     | [1.76, 1.16, 0.73] | 2.1051                 | 23.42   |
| 4     | [2.55, 1.15, 0.73] | 2.5555                 | 7.09    |
| 5     | [2.63, 1.15, 0.72] | 2.6056                 | 5.25    |
| 6     | [2.81, 1.15, 0.72] | 2.7036                 | 1.69    |

$$A = \begin{pmatrix} 0.5 & 0.1 & 0.2 \\ 0.1 & 0.6 & 0.1 \\ 0.2 & 0.1 & 0.7 \end{pmatrix} \text{ and } \vec{b} = \begin{pmatrix} 0 \\ 1 \\ 0 \end{pmatrix}$$
 (3)

respectively. Again,  $\vec{b}$  is normalized for qutrit states, and can be directly encoded as  $|b\rangle = |1\rangle$ . This state can be achieved using a single qutrit increment gate. The statevector results obtained for this calculation using qutrit HHL for different values of  $n_r$  are given in Table II.

Table II: Results from executing the qutrit HHL algorithm for the toy A matrix and  $\vec{b}$  described in equation (3), for different numbers of QPE clock register qutrits.

| $\overline{n_r}$ | $ec{x}$              | $ \langle b x\rangle $ | PFD (%) |
|------------------|----------------------|------------------------|---------|
| 2                | [-0.25, 1.69, -0.16] | 1.69272                | 2.80    |
| 3                | [-0.28, 1.71, -0.15] | 1.70506                | 2.10    |
| 4                | [-0.28, 1.73, -0.16] | 1.72855                | 0.75    |
| 5                | [-0.29, 1.73, -0.19] | 1.73218                | 0.54    |

#### B. Quantum chemistry simulations

We now move on to results from our simulations for quantum chemistry. We consider the  $H_2$  molecule in the 6-31G basis with different bond lengths (9 data points between 1.2 and 1.6 Bohr) to obtain a potential energy curve (PEC). For each geometry considered, the system includes four molecular orbitals that comprise one occupied and three virtuals. The outermost virtual molecular orbital is frozen, hence our calculations consist of only three molecular orbitals for our active space that equals six spin orbitals. We use the GAMESS-US software [24] to generate the configuration interaction Hamiltonian in the singles and doubles approximation (CISD). In particular, we use Graphical unitary group approach (GUGA)-CISD so that the size of the Hamiltonian matrix reduces

to  $4 \times 4$ . Since the A matrix obtained using linearized coupled cluster method in the singles and doubles approximation (LCCSD) is a principal sub-matrix of the Hamiltonian matrix, where we slice away the first row and first column (which is  $\vec{b}$ ) of the latter [8], the state register in HHL has only one qutrit. We benchmark our results with energies obtained using the LCCSD approximation and CISD on a classical computer. On the HHL front, the one-qutrit isometry circuit for each bond length is a rotation gate,  $R_{02}(\theta)$ , with the choice of rotation angle depending on the bond length. Table A.1 of Appendix presents the values chosen for  $\theta$ .

The PEC is presented in Figure 5, and the accompanying data is presented in Table A.2 of the Appendix. Throughout,  $n_r$  is set to 5 for our qutrit HHL calculations, while for the qubit HHL computations, we set  $n_r = 8$  to capture the results with comparable precision. However, for completeness, we also present the PEC with  $n_r = 5$  for qubit HHL in the figure as well as the table. We also add that many works that present quantum chemistry results in the quantum computing framework quote their methods' energies relative to a benchmark value, but such a presentation does not provide complete context on how well an approach has captured correlation effects, given that one almost always starts with a reference wave function like the HF state to build the more accurate one and compute energies. Therefore, we also present the HF energies in the PEC as well as in the table of results, except that in Figure 5 we shift the HF energy at each bond length value, R, by a constant number for visual ease of discerning the total energy values provided using qubit HHL, gutrit HHL, LCCSD, and CISD methods. This is due to the fact that the correlation energy is typically much much smaller than the total energy or for that matter the HF energy, and therefore when we provide the HF energy in a figure along with the correlated values from methods like LCCSD, CISD, qubit HHL and qutrit HHL, one fails to discern the latter points. Our results show that as expected, gutrit HHL-LCCSD computations are able to capture correlation effects reasonably well, and the results are at most to within 0.02 percent of the classical LCCSD value.

We now focus on the equilibrium geometry obtained from our PEC (1.4 Bohr), to study the effect of  $n_r$  on the correlation energy using qubit and qutrit HHL implementations. The results are provided in Figure 6, with Table A.3 of the Appendix presenting the accompanying data. We stop at  $n_r = 6$  in the figure due to computational limitations from qutrit HHL. We note that for the purposes of our statevector calculations, setting  $n_r = 6$  would result in  $2^6 = 64$  multi-controlled rotation gates in the controlled-rotation module in the case of qubits, whereas

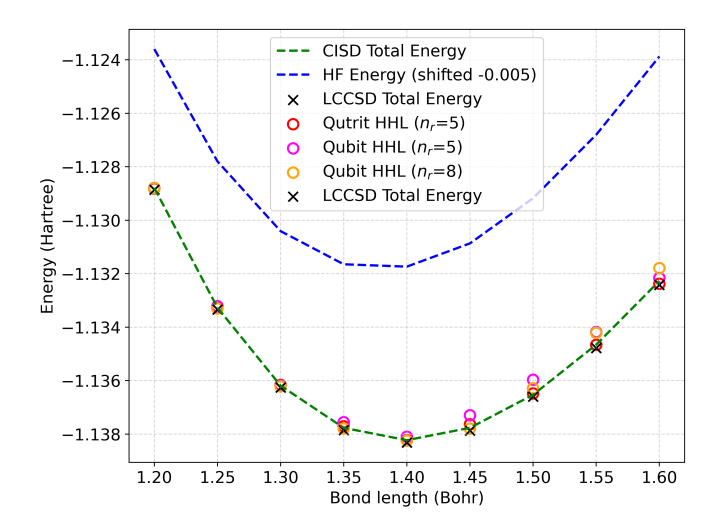


Figure 5: Potential energy curves with energies specified in units of Hartree for the  $H_2$  molecule. The HF energies have each been shifted by an amount of -0.005 Hartree for ease of visual representation.

for autrits, we end up with  $3^6 = 729$  multi-controlled rotation gates. This observation underscores the need to develop more computationally efficient classical computing routines for qudit HHL implementations in general, and we defer the exercise for a future study. We now turn our attention back to the results in Figure 6, which show that for a fixed number of qudits in the clock register, qutrit HHL performs much better than its qubit counterpart. This is not surprising, given that the eigenvalues are captured to  $3^{n_r}$  precision for gutrits, whereas it is  $2^{n_r}$ for qubits. We also see that 'convergence' to the expected correlation energy value is achieved faster for gutrit HHL than qubit HHL for the same reason. We recall that the HHL algorithm involves a constant C (introduced in Section IIIC). We have modified this constant as by taking its ternary expansion (for qutrits) and its binary expansion (for qubits) up to the same precision as is achieved by the number of qudits in the clock register. Figure 6 shows that the correlation energies have improved with the ternary and binary expanded C values for qubit and qutrit HHL respectively.

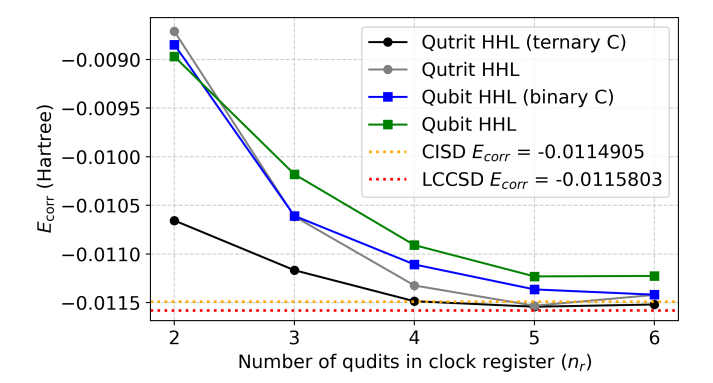


Figure 6: Correlation energy in Hartree for the  $H_2$  molecule with equilibrium bond length, obtained from statevector simulations of the qubit and qutrit HHL algorithms with different values for  $n_r$ .

# VI. COMPARISON OF QUBIT AND QUTRIT HHL

### A. Analyzing the number of qudits

We analyze the number of qubits and qutrits required for a given precision.

## 1. Clock register:

Let the required precision in decimal numbers be p digits. This means that we want the error to be  $\epsilon=10^{-p}$ . In the previous sections, the number of qudits in this register are denoted by  $n_r$ . Since the captured eigenvalues  $|\phi\rangle$  are stored in these  $n_r$  qudits as  $|\tilde{\phi}\rangle$ ,  $|\phi-\tilde{\phi}|=\frac{1}{d^{n_r}}$ , where d is the dimension of the qudit. In such a case, the maximum error  $\epsilon$  will be  $\frac{1}{d^{n_r}}$ , and hence

$$10^{-p} = \epsilon = \frac{1}{d^{n_r}}$$
$$d^{n_r} = 10^p$$
$$n_r = p \log_d(10).$$

Henceforth, we shall use  $n_r^{(t)}$  for qutrits and  $n_r^{(b)}$  for qubits. For qubits, d=2, and hence

$$n_r^{(b)} = p \log_2(10),$$
 (4)

while for qutrits, d = 3, and therefore

$$n_r^{(t)} = p \log_3(10)$$

$$n_r^{(t)} = p \frac{\log_2(10)}{\log_2(3)}$$

$$n_r^{(t)} = \frac{n_r^{(b)}}{\log_2(3)}.$$
(5)

Thus, the number of qutrits required in the clock register is lesser by a factor of  $log_2(3)$  as compared to qubits. That is -

$$n_r^{(t)} = \frac{n_r^{(b)}}{\log_2(3)} \approx 0.63 \ n_r^{(b)}.$$
 (6)

For qudits in general, the reduction is by a factor of  $log_2(d)$  as compared to qubits.

### 2. State register:

In order to encode the  $N \times 1$  dimensional  $\vec{b}$  in the state register, m qudits are required such that  $N \leq d^m$ . Since we work in the binary (for qubits) and the ternary (for qutrits) frameworks, the size of  $|b\rangle$  is accordingly  $2^{m^{(b)}}$  or  $3^{m^{(t)}}$ . Here,  $m^{(b)}$  and  $m^{(t)}$  represent the number of qubits and qutrits in the state register respectively. The  $\vec{b}$  must be encoded in these quantum states, and hence  $m^{(b)}$  or  $m^{(t)}$  are chosen such that they accommodate the  $N \times 1$  dimensional  $\vec{b}$ , while the remaining  $d^m - N$  entries are taken as zeroes. From this condition, it can be shown that

$$m > loq_d(N),$$

and the relation between the number of qubits and qutrits follows from this as

$$m^{(t)} \approx \frac{m^{(b)}}{loq_2(3)} \approx 0.63 m^{(b)}.$$
 (7)

Once again, we see a suppression in the number of qutrits in the state register by a factor of  $log_2(3)$ . This is a general expression, but for our quantum chemistry application, we can arrive at estimates for the number of qubits and qutrits in terms of the number of spin orbitals,  $N_s$ . For an LCCSD computation, the number of possible single and double excitations scale at most as  $N_s^4$ , which is the length of the original  $\vec{b}$ . For encoding it in a qubit or qutrit space, we need to pad these with zeroes until we reach a size of  $2^{m^{(b)}}$  (for qubits) or  $3^{m^{(t)}}$  (for

qutrits). Table III shows how the state register size grows with increasing  $N_s$ . We immediately see that for a calculation involving 20 spin orbitals, we need 18 qubits on the state register, whereas in a qutrit HHL implementation, we need 13.

Table III: A comparison of the number of qubits and qutrits required in the state register for the LCCSD problem.  $N_s$  is the number of spin orbitals resulting in  $N_s^4$  possible excitations. For a given precision, the number of qubits and qutrits required are  $m^{(b)}$  and  $m^{(t)}$  respectively.

| $N_s$ | $N_s^{4}$ | $2^{m^{(b)}}$ | $m^{(b)}$ | $3^{m^{(t)}}$ | $m^{(t)}$ |
|-------|-----------|---------------|-----------|---------------|-----------|
| 2     | 16        | 16            | 4         | 27            | 3         |
| 4     | 256       | 256           | 8         | 729           | 6         |
| 6     | 1296      | 2048          | 11        | 2187          | 7         |
| 8     | 4096      | 4096          | 12        | 6561          | 8         |
| 10    | 10000     | 16384         | 14        | 19683         | 9         |
| 12    | 20736     | 32768         | 15        | 59049         | 10        |
| 14    | 38416     | 65536         | 16        | 177147        | 11        |
| 16    | 65536     | 65536         | 16        | 177147        | 11        |
| 18    | 104976    | 131072        | 17        | 531441        | 12        |
| 20    | 160000    | 262144        | 18        | 1594323       | 13        |

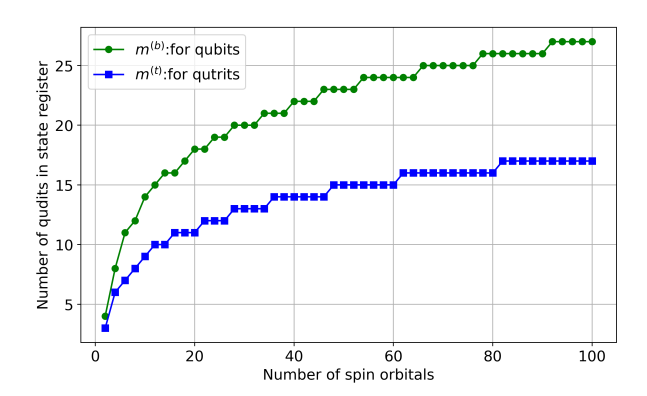


Figure 7: A comparison of the number of qubits and qutrits required in the state register for the HHL-LCCSD problem.

Figure 7 gives a graphical representation of a similar comparison up to  $N_s = 100$ .

## 3. HHL ancilla:

A single qudit is required for the HHL ancilla regardless of it being a qubit or a qutrit.

Thus, in the gutrit HHL implementation,

$$\label{eq:polynomial} \text{Total number of qutrits} \approx p \frac{log_2(10)}{log_2(3)} + \frac{log_2(N)}{log_2(3)} + 1,$$

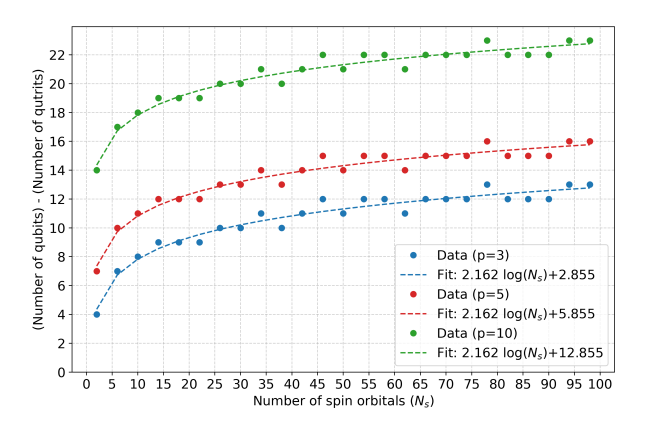


Figure 8: Curves showing the difference in the number of qubits and qutrits required for a given precision p, specific for the HHL-LCCSD problem.

as compared to the qubit HHL implementation, where

Total number of qubits  $\approx p \log_2(10) + \log_2(N) + 1$ .

Figure 8 gives a visual representation of the difference in the total number of qutrits and qubits required for the HHL implementations with a given precision. We have done curve-fitting for three different values of precision. It can be seen from the plot that the number of qutrits required is lesser than qubits by a logarithmic amount, and that the difference increases with a demand for better precision. We add that since one needs to extract a feature of  $|x\rangle$  post-HHL, which in our case is the overlap  $|\langle b|x\rangle|$ , the appended controlled-swap circuit module requires preparing an additional  $|b\rangle$ , and thus fewer qutrits than qubits as discussed earlier in the state register qudit count part.

### B. Analyzing the number of 2-qudit gates

The overall resource cost can be estimated by the number of two-qudit gates, since they are considered to be the major sources of error at the physical level. We do the counting module-wise as follows:

## 1. Controlled-unitaries within QPE:

The total number of controlled-unitaries for qubits is  $2^{n_r^{(b)}} - 1$ , while for qutrits it is  $\frac{1}{2}(3^{n_r^{(t)}} - 1)$ . However, for a given precision p, using equation 5,

we can show that

$$3^{n_r^{(t)}} = 3^{\frac{n_r^{(b)}}{\log 2(3)}}$$

$$= 3^{n_r^{(b)} \log_3(2)}$$

$$= (3^{\log_3(2)})^{n_r^{(b)}}$$

$$= 2^{n_r^{(b)}}.$$
(8)

Therefore, the number of controlled-unitaries is halved for the qutrit case. We now assume a recursive decomposition scheme for the  $m^{(b)}$  qubits in the state register as proposed in Reference [25], and a similar decomposition scheme for the  $m^{(t)}$  qutrits [26], and work out both the cases to find that the number of two-qudit gates are of the same order. This is achieved because of the fact that for a given precision  $m^{(b)}$  and  $m^{(t)}$  are related using equation 7. We note that while the decomposition for qubits goes as  $4^{m^{(b)}}$  and the one for qutrits scales as  $9^{m^{(t)}}$ , the number of two-qudit gates in a controlled-unitary gate scales quadratically in the A matrix size due to amplitude encoding in both the cases.

### 2. IQFT module within QPE:

The count for two-qudit gates in this module is  $\frac{n_r^{(b)^2}-1}{2}$  for qubits and  $\frac{n_r^{(t)^2}-1}{2}$  for qutrits, which can be simplified using equation 6 as  $\approx \frac{0.39 \ n_r^{(b)^2}-1}{2}$ . Therefore, the IQFT module with qutrits has  $\approx 39\%$  gates as its qubit counterpart.

## 3. Controlled-rotation module:

The number of multi-controlled rotation gates for the controlled rotation module is  $d^{n_r}$ . This means that qutrit HHL requires  $3^{n_r}$  multi-controlled rotations and qubit HHL requires  $2^{n_r}$  multi-controlled rotations. Using equation 8, we can show that the number of multi-controlled rotation gates in the controlled-rotation module is equal for both the qubit and qutrit HHL implementations. The decomposition to two-qudit gates again goes as in the first point. Hence, the number of two-qudit gates in the controlled-rotation module are comparable for both the implementations.

### VII. CONCLUSION

In this work, we extend the HHL algorithm from its qubit form to the qutrit framework, by designing the circuit (including a simplified controlled-rotation module) as well as developing qubit and qutrit HHL codes in the BQSKit framework. To demonstrate the working of the qutrit HHL algorithm, we carry out toy matrix calculations as well as quantum chemical calculations to generate the potential energy curve of the model  $H_2$  molecule. We obtain correlation energies to within 0.02 percent precision for the latter, and also benchmark our results with CISD and LCCSD calculations using classical methods.

We report the following observations in contrast with the qubits case: we show that for a given precision, the required number of clock register qutrits is lower by a factor of  $log_2(3)$  relative to qubit HHL; it goes as  $log_2(d)$ for qudit HHL in general. To amplitude encode the same amount of information from the  $N \times 1$  vector,  $\vec{b}$ , into the HHL input state, we observe that number of gutrits required is  $\lceil \log_3(N) \rceil$  while for qubits it is  $\lceil \log_2(N) \rceil$ . With regard to the number of 2-qudit gates, the requirement for the QFT module within QPE is reduced to 39% of the number of 2-qubit gates needed in qubit HHL, whereas the number of controlled unitaries in the QPE module reduces to 50% of those necessary for qubit HHL. The number of multi-controlled rotation gates in the controlledrotation module is found to be the same in both cases. However, when we decompose each controlled-unitary, and multi-controlled rotation gate in terms of 2-qudit gates, we find that the 2-qudit gate count for qubit and qutrit HHL is comparable. Overall, we conclude that if one is able to realize quantum hardware with good quality qutrits, a qutrit HHL implementation is relatively cheaper in the number of qudits, while the number of gates is comparable for both qubit and qutrit HHL implementations.

### ACKNOWLEDGMENTS

VSP acknowledges support from CRG grant (CRG/2023/002558). TP and VSP thank Dr. Akshaya Jayashankar for her constant support with conceptual ideas throughout the duration of the work. TP thanks Ms. Aashna Zade for her help with GAMESS, and Mr. Peniel Bertrand Tsemo for discussions on quantum chemistry. TP and VSP thank Dr. Ed Younis for his support with BQSKit, and thank their group members for reading the manuscript and giving their comments (Aashna, Peniel, Disha, Fazil, Akshaya, Smriti and Kalam).

# **APPENDIX**

Table A.1:  $\theta$  (in radians and rounded off to four decimal places) used to implement the isometry module in qutrit HHL for every bond length (R) in Bohr, for the PECs in Figure 5.

| R        | 1.20   | 1.25   | 1.30   | 1.35   | 1.40   | 1.45   | 1.50   | 1.55   | 1.60   |
|----------|--------|--------|--------|--------|--------|--------|--------|--------|--------|
| $\theta$ | 1.0296 | 1.0074 | 0.9845 | 0.9615 | 0.9383 | 0.9152 | 0.8920 | 0.8690 | 0.8465 |

Table A.2: Table showing the data for all the relevant energy values used for generating the PECs in Figure 5. All the energies are specified in units of Hartree and bond lengths are in units of Bohr. All the energies are rounded off to the sixth decimal place.

| $\overline{R}$ | $E_{\mathrm{HF}}$ | $E_{\text{CISD}}$         | $E_{\text{LCCSD}}$         | $E_{\text{qutrit HHL}}$ with $n_r = 5$ | $E_{\text{qubit HHL}}$ with $n_r = 5$ | $E_{\text{qubit HHL}}$ with $n_r = 8$  |
|----------------|-------------------|---------------------------|----------------------------|--|---------------------------------------|--|
|                |                   | $(E_{ m CISD}^{ m corr})$ | $(E_{ m LCCSD}^{ m corr})$ | $(E_{ m qutrit\ HHL}^{ m corr})$       | $(E_{ m qubit\ HHL}^{ m corr})$       | $(E_{\text{qubit HHL}}^{\text{corr}})$ |
| 1.20           | -1.118598         | -1.128792                 | -1.128855                  | -1.128816                              | -1.128795                             | -1.128798                              |
|                |                   | (-0.010194)               | (-0.010257)                | (-0.010218)                            | (-0.010197)                           | (-0.010199)                            |
| 1.25           | -1.122798         | -1.133270                 | -1.133338                  | -1.133287                              | -1.133218                             | -1.133305                              |
|                |                   | (-0.010472)               | (-0.010540)                | (-0.010489)                            | (-0.010420)                           | (-0.010507)                            |
| 1.30           | -1.125408         | -1.136187                 | -1.136261                  | -1.136163                              | -1.136192                             | -1.136217                              |
|                |                   | (-0.010779)               | (-0.010853)                | (-0.010755)                            | (-0.010785)                           | (-0.010809)                            |
| 1.35           | -1.126649         | -1.137766                 | -1.137847                  | -1.137709                              | -1.137556                             | -1.137791                              |
|                |                   | (-0.011117)               | (-0.011198)                | (-0.011061)                            | (-0.010907)                           | (-0.011143)                            |
| 1.40           | -1.126737         | -1.138228                 | -1.138317                  | -1.138227                              | -1.138101                             | -1.138246                              |
|                |                   | (-0.011491)               | (-0.011580)                | (-0.011490)                            | (-0.011364)                           | (-0.011509)                            |
| 1.45           | -1.125866         | -1.137766                 | -1.137865                  | -1.137636                              | -1.137297                             | -1.137797                              |
|                |                   | (-0.011900)               | (-0.011999)                | (-0.011770)                            | (-0.011431)                           | (-0.011930)                            |
| 1.50           | -1.124177         | -1.136529                 | -1.136601                  | -1.136480                              | -1.135970                             | -1.136288                              |
|                |                   | (-0.012352)               | (-0.012424)                | (-0.012303)                            | (-0.011794)                           | (-0.012111)                            |
| 1.55           | -1.121802         | -1.134653                 | -1.134780                  | -1.134663                              | -1.134182                             | -1.134214                              |
|                |                   | (-0.012851)               | (-0.012978)                | (-0.012861)                            | (-0.012380)                           | (-0.012412)                            |
| 1.60           | -1.118877         | -1.132271                 | -1.132414                  | -1.132379                              | -1.132160                             | -1.131793                              |
|                |                   | (-0.013394)               | (-0.013537)                | (-0.013502)                            | (-0.013283)                           | (-0.012917)                            |
|                |                   |                           |                            |  | ·                                     |  |

Table A.3: Correlation energies in units of Hartree obtained with different values of  $n_r$  (the number of clock register qudits) for the  $H_2$  molecule with equilibrium bond length, from statevector simulations of the qubit and qutrit HHL implementations. The LCCSD and the CISD values for the correlation energies are provided for reference. All the energies are rounded off to the sixth decimal place. C is the minimum eigenvalue of A, while binary and ternary C are its binary and ternary expansions to a precision of  $n_r$  qubits and qutrits respectively.

| $n_r$ |           | $E_{corr}^{(b)}$ |           | $E_{corr}^{(t)}$ |  |  |
|-------|-----------|------------------|-----------|------------------|--|--|
|       | With C    | With binary C    | With C    | With ternary C   |  |  |
| 2     | -0.008970 | -0.008848        | -0.008712 | -0.010656        |  |  |
| 3     | -0.010180 | -0.010608        | -0.010613 | -0.011167        |  |  |
| 4     | -0.010908 | -0.011107        | -0.011323 | -0.011485        |  |  |
| 5     | -0.011230 | -0.011364        | -0.011531 | -0.011542        |  |  |
| 6     | -0.011225 | -0.011418        | -0.011420 | -0.011519        |  |  |
| LCCSD | -0.011580 |                  |           |                  |  |  |
| CISD  | -0.011490 |                  |           |                  |  |  |

- A. W. Harrow, A. Hassidim, and S. Lloyd, Physical Review Letters 103, 150502 (2009).
- [2] R. Yalovetzky, P. Minssen, D. Herman, and M. Pistoia, Scientific Reports 14, 20610 (2024).
- [3] Y. Tan, H. Kukina, and J. Szefer, in 2024 IEEE 6th International Conference on Trust, Privacy and Security in Intelligent Systems, and Applications (TPS-ISA) (IEEE, 2024) pp. 481–488.
- [4] M. Gopalakrishnan Meena, K. C. Gottiparthi, J. G. Lietz, A. Georgiadou, and E. A. Coello Pérez, Physics of Fluids 36, 10 (2024).
- [5] P. Pareek, A. Jayakumar, C. Coffrin, and S. Misra, arXiv preprint arXiv:2402.08617 (2024).
- [6] W. Robson, K. K. Saha, C. Howington, I.-S. Suh, and J. Nabrzyski, in 2022 IEEE International Conference on Quantum Computing and Engineering (QCE) (IEEE, 2022) pp. 741–744.
- [7] N. Baskaran, A. S. Rawat, A. Jayashankar, D. Chakravarti, K. Sugisaki, S. Roy, S. B. Mandal, D. Mukherjee, and V. Prasannaa, Physical Review Research 5, 043113 (2023).
- [8] P. B. Tsemo, A. Jayashankar, K. Sugisaki, N. Baskaran, S. Chakraborty, and V. Prasannaa, Physical Review Research 7, 023270 (2025).
- [9] S.-H. Chiew and L.-C. Kwek, arXiv preprint arXiv:2302.06638 (2023).
- [10] A. Peruzzo, J. McClean, P. Shadbolt, M.-H. Yung, X.-Q. Zhou, P. J. Love, A. Aspuru-Guzik, and J. L. O'brien, Nature Communications 5, 4213 (2014).
- [11] A. Aspuru-Guzik, A. D. Dutoi, P. J. Love, and M. Head-Gordon, Science 309, 1704 (2005).
- [12] Peniel Bertrand Tsemo and V. S. Prasannaa (private communication, 2025).
- [13] S. Yang, L. Xu, G. Tian, and X. Sun, arXiv preprint arXiv:2504.12710 (2025).

- [14] A. Morvan, V. V. Ramasesh, M. S. Blok, J. M. Kreikebaum, K. O'Brien, L. Chen, B. K. Mitchell, R. K. Naik, D. I. Santiago, and I. Siddiqi, Physical Review Letters 126, 210504 (2021).
- [15] Y. Wang, Z. Hu, B. C. Sanders, and S. Kais, Frontiers in Physics 8, 589504 (2020).
- [16] S. Reddy, Journal of Applied Physics 135 (2024).
- [17] Y. Saxena, S. Chatterjee, and T. Sapv, arXiv preprint arXiv:2504.15265 (2025).
- [18] M. Sawerwain and W. Leonski, arXiv preprint arXiv:1309.0800 (2013).
- [19] A. Zaman, H. J. Morrell, and H. Y. Wong, IEEE Access 11, 77117 (2023).
- [20] D. Gottesman, in NASA International Conference on Quantum Computing and Quantum Communications (Springer, 1998) pp. 302–313.
- [21] We clarify that we use the term 'linearized coupled cluster' in the context of Ref. [7], and not in the same context as Ref. [?].
- [22] H. Buhrman, R. Cleve, J. Watrous, and R. De Wolf, Quantum fingerprinting (2001).
- [23] E. Younis, C. C. Iancu, W. Lavrijsen, M. Davis, and E. Smith, Berkeley quantum synthesis toolkit (BQSKit) v1, Tech. Rep. (Lawrence Berkeley National Laboratory (LBNL), Berkeley, CA (United States), 2021).
- [24] G. M. J. Barca et al., J. Chem. Phys. 152, 154102 (2022).
- [25] V. V. Shende, S. S. Bullock, and I. L. Markov, in Proceedings of the 2005 Asia and South Pacific Design Automation Conference (2005) pp. 272–275.
- [26] G.-L. Jiang, W.-Q. Liu, and H.-R. Wei, arXiv preprint arXiv:2310.11996 (2023).